Mathematical Biosciences and Engineering

MBE, 18(5): 5592–5613.
DOI: 10.3934/mbe.2021282
Received: 11 May 2021
Accepted: 11 June 2021
Published: 22 June 2021

http://www.aimspress.com/journal/MBE

Theory article

Conjugated heat transfer of power-law fluids in double-pass concentric circular heat exchangers with sinusoidal wall fluxes

Chii-Dong Ho [1,*], Gwo-Geng Lin [1], Thiam Leng Chew [2,3] and Li-Pang Lin [1]

[1] Department of Chemical and Materials Engineering, Tamkang University, 151 Yingzhuan Road, Tamsui, New Taipei, Taiwan 251
[2] Department of Chemical Engineering, Faculty of Engineering, Universiti Teknologi Petronas, 32610 Seri Iskandar, Perak Darul Ridzuan, Malaysia
[3] CO2 Research Center (CO2RES), Institute of Contaminant Management, Universiti Teknologi Petronas, 32610 Seri Iskandar, Perak Darul Ridzuan, Malaysia

* **Correspondence:** Email: cdho@mail.tku.edu.tw; Tel: +1-886-2-2621-5656 ext. 2724; Fax: +1-886-2-2620-9887.

Abstract: An analytical formulation, referred to as conjugated Graetz problems, is developed to predict the temperature distribution and Nusselt numbers for the power-law fluid flowing in a double-pass concentric circular heat exchanger under sinusoidal wall fluxes. A new design of inserting an impermeable sheet into a concentric tube, in parallel, to conduct recycling double-pass operations has been studied theoretically in the fully developed region, resulting in substantial improvements in the performance of heat exchanger device. The analytical solution was derived using the complex functions by transforming the boundary value problem into ordinary differential equations with the aid of the Frobenius method. The influences of power-law index and impermeable-sheet position on average Nusselt numbers with various designs and operating parameters are also delineated. The theoretical predictions show that the heat transfer efficiency is considerably improved through operating the double-pass device compared to via a single-pass circular heat exchanger (where an impermeable sheet is not inserted). The economic feasibility of operating double-pass concentric circular heat exchanger for power-law fluids is exemplified by the ratio of the heat-transfer efficiency enhancement and the increment in power consumption. The double-pass effect from increasing the convective heat-transfer coefficient can compensate for the rise in power consumption, which serves as important economic advantage of this design.

Keywords: power-law fluids; sinusoidal wall fluxes; concentric circular heat exchangers; conjugated

Graetz problem

1. Introduction

A wide variety of heat-transfer problems applied to Newtonian fluids flow in bounded conduits of cylindrical or parallel-plate geometries with negligible axial conduction has been successfully reduced and known as the Graetz problem [1,2]. Multi-stream or multiphase systems, however, are fundamentally different since conjugated boundary conditions must be coupled at the boundaries, referred to as conjugated Graetz problems [3,4], which were solved analytically by means of an orthogonal expansion technique [5,6] with the eigenfunction expansion in terms of the extended power series. Extension to markedly increased applications of practical processes with recycle-effect concept is possible. It's been widely used in separation, fermentation, and polymerization such as distillation [7], extraction [8], loop reactors [9], air-lift reactor [10], draft-tube bubble column [11], mass exchanger [12], and thermal diffusion column [13].

Many materials of food, polymeric systems, biological process, pulp and paper suspensions [14] with high molecular weight in processing industries exhibit a range of non-Newtonian fluid behavioral features and display shear-thinning and/or shear thickening behavior [15,16]. Those non-Newtonian fluids can be treated as the laminar flow conditions with negligible viscoelastic effects based on their high viscosity levels in the appropriate shear rate range [17]. Therefore, the analytical solution could be analogously obtained under the similar mathematical treatment when dealing with Newtonian fluids. A considerable body of literature has shown the practical feasibility of solving the power-law model of non-Newtonian flows by LBM (Lattice Boltzmann Method). It is also devoted to studying the non-Newtonian behavior with shear-thinning and shear-thickening liquids on sedimentation [18,19] and flows over a heated cylinder [20], an inclined square [21], cylinder [22] and various shapes [23]. Furthermore, the heat-transfer responses to the distributions of the conduit wall and fluid temperature are two major concerns in investigating the heat-transfer efficiency improvement under different kinds of boundary conditions which can be detected at the conduit wall. Two cases of the uniform wall temperature (Dirichlet problem) [24, 25] and uniform heat flux (Neumann problem) [26,27] were processed in the application of engineering field, in general. Recently, a non-trivial amount of research use metal foams of PCMs (phase change materials) and nanoparticles of NEPCMs (nano-encapsulated phase change materials) to enhance heat transfer properties in some applications regarding constant heat load, transient, or cyclic loads. Thermal and energy storage managements of crucial importance of systems were investigated within the thermal performance given variable heat loads [28] and non-uniform magnetic sources [29], as well as thermal benefit of NEPCMs nanoparticles in microchannels that considers forced convection [30] and natural convection flow [31,32]. However, the well-known case of sinusoidal wall heat flux distribution [33] of non-uniform heating was the simplest model of period heating within the convective heat-transfer problems in the periodic [34] and circumferentially [35] heating systems. It's been investigated by many researchers to design the cooling tubes in nuclear reactors [36].

The present study is an extension of our previous work [37] to apply the system of non-Newtonian fluids for the conjugated Graetz problem where the power-law index of the shearing-thinning aqueous polymer solutions were given. Though the phenomenon of heat transfer in the present study could be drawn parallel comparison, in similar sense, with that of heat-transfer mechanism in our previous

work [37], the manners of non-Newtonian fluids with the convective heat transfer are somehow different. It's actually affected by the velocity profile of shear-thinning fluid. A power-law fluid flowing through a double-pass laminar countercurrent-flow concentric-tube heat exchanger that implemented an impermeable sheet with sinusoidal wall fluxes was investigated for the purpose of examining the heat transfer efficiency and temperature distributions under external recycling, which was solve analytically through the resultant conjugated partial differential equations by the superposition technique. The recycle ratio and impermeable-sheet position are two parameters treated as essential and should be suitably adjusted to an improved design of heat transfer equipment. The comparison of heat-transfer efficiency improvement and Nusselt numbers in both operations (single- and double-pass device) is also discussed.

2. Dimensionless temperature distributions

A double-pass concentric circular heat exchanger was made by inserting an impermeable sheet into a circular tube of inside diameter $2R$ and length L, as shown in Figure 1. The thickness of the inner (subchannel a) and annular tube (subchannel b) are $2\kappa R$ and $2(1\text{-}\kappa)R$, respectively. Comparing with the radius of outer circular tube R and outer circular tube R_1, the thickness of the impermeable barrier δ is negligible ($\delta << R$). Two flow patterns, flow pattern A and flow pattern B, are proposed by and used in this study. An inlet fluid with volumetric flow rate V and temperature T_1 will enter the subchannel a and then flows reversely into the subchannel b with the aid of a convectional pump at the end of the conduit like flow pattern A, as shown in Figure 1(a). On the other hand, the flow pattern B is that the fluid feeds into subchannel b and exits from the subchannel a, as shown in Figure 1(b). The fluid is heated by the outer wall with sinusoidal heat fluxes, $q_w''(z) = q_0''[1 + sin(\beta z)]$ in both flow patterns.

The problem of laminar heat transfer at steady state with negligible axial conduction was known as the Graetz problem, and the convective velocity in radial direction is neglected by applying the Navier-stokes relations to obtain the hydro-dynamical equation for laminar flow. The energy balance equations of fluid flowing in the subchannel a and subchannel b in dimensional form with specified velocities are:

$$\rho C_p v_a(r) \frac{\partial T_a(r,z)}{\partial z} = \frac{k}{r}\frac{\partial}{\partial r}\left(r\frac{\partial T_a(r,z)}{\partial r}\right) + k\frac{\partial^2 T_a}{\partial z^2} \tag{1}$$

$$\rho C_p v_b(r) \frac{\partial T_b(r,z)}{\partial z} = \frac{k}{r}\frac{\partial}{\partial r}\left(r\frac{\partial T_b(r,z)}{\partial r}\right) + k\frac{\partial^2 T_b}{\partial z^2} \tag{2}$$

The theoretical analysis of double-pass heat exchangers is developed based on the following assumptions: (a) constant physical properties of fluid; (b) fully-developed laminar flow with power law index ω ($\tau = -c\,\dot{\gamma}^{\omega}$) in each subchannel; (c) neglecting the entrance length and the end effects; (d) ignoring the longitudinal heat conduction and the thermal resistance of the impermeable sheet; (e) well mixed at both inlet and outlet. With these assumptions, the dimensionless energy balance equations and the velocity distributions of a double-pass heat exchanger with sinusoidal heat fluxes were formulated by neglecting the second terms on the right-hand side of Eq. (1) and Eq. (2). The descriptions of two or more contiguous streams of multi-stream (or phases of multi-phase) problems with coupling mutual boundary conditions [38,39] becomes

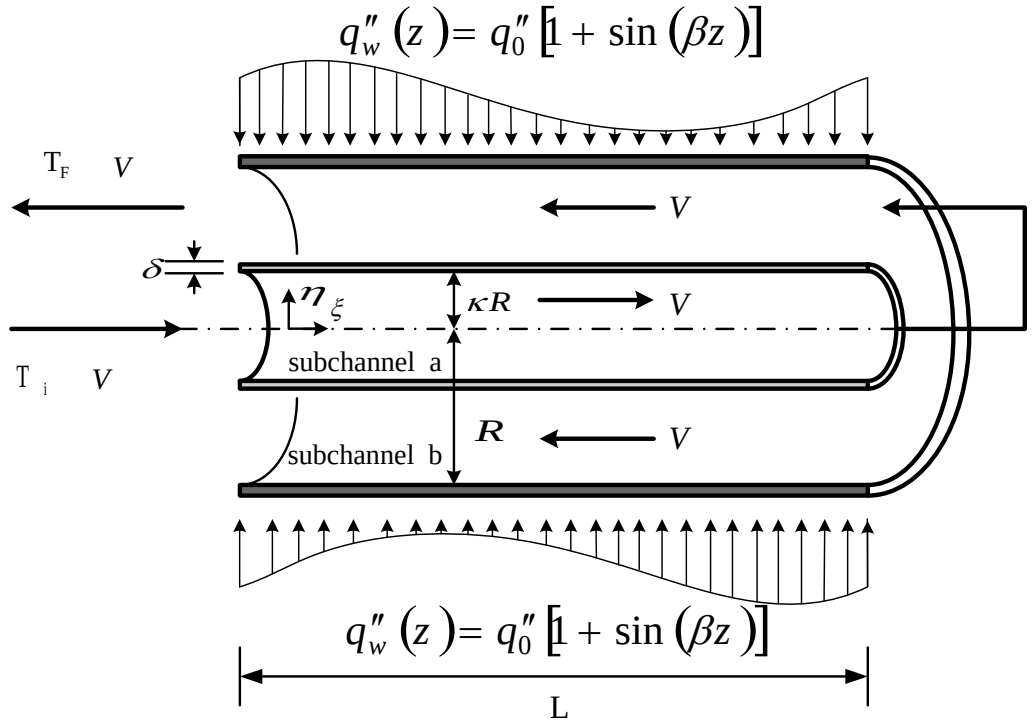

(a) Flow pattern A

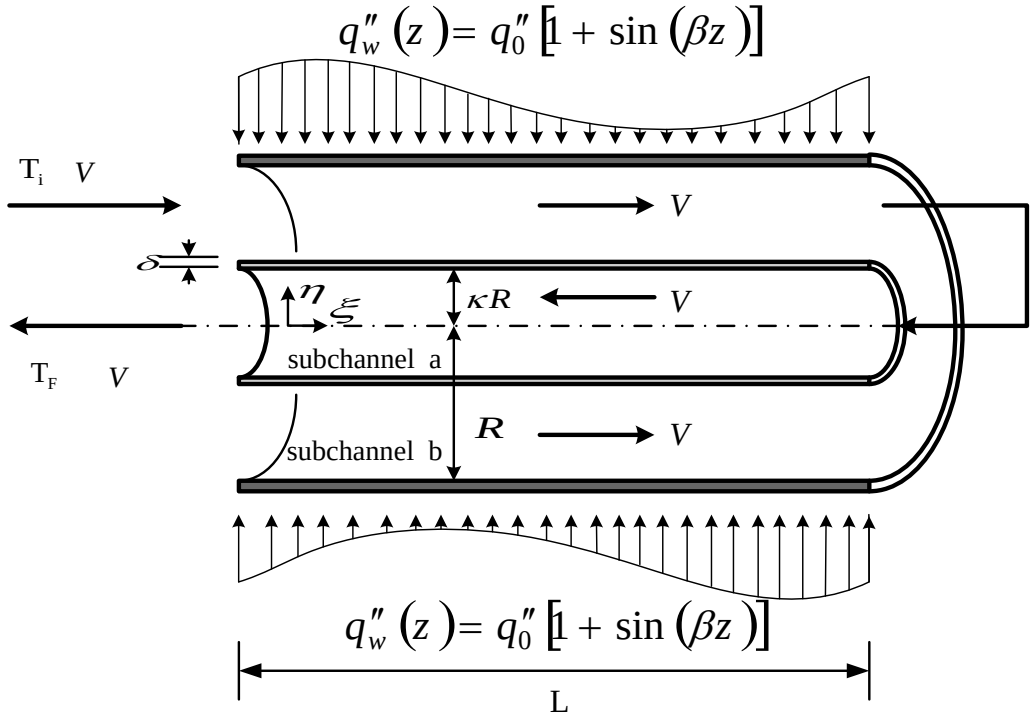

(b) Flow pattern B

Figure 1. Schematic diagram of a double-pass concentric circular heat exchanger.

$$\left(\frac{v_a(\eta)R^2}{\alpha GzL}\right)\frac{\partial\varphi_a(\eta,\xi)}{\partial\xi}=\frac{1}{\eta}\frac{\partial}{\partial\eta}\left(\eta\frac{\partial\varphi_a(\eta,\xi)}{\partial\eta}\right) \tag{3}$$

$$\left(\frac{v_b(\eta)R^2}{\alpha GzL}\right)\frac{\partial\varphi_b(\eta,\xi)}{\partial\xi}=\frac{1}{\eta}\frac{\partial}{\partial\eta}\left(\eta\frac{\partial\varphi_b(\eta,\xi)}{\partial\eta}\right) \tag{4}$$

where v_a and v_b are the velocity distributions in subchannels a and b, respectively, as follows in flow pattern A:

$$v_a=\left(\frac{3\omega+1}{\omega+1}\right)\frac{V}{\pi(\kappa R)^2}\left(1-\left(\frac{\eta}{\kappa}\right)^{\frac{\omega+1}{\omega}}\right)=G\left(1-\left(\frac{\eta}{\kappa}\right)^{\frac{\omega+1}{\omega}}\right),\quad 0\le\eta\le\kappa \tag{5}$$

$$v_b=-\frac{(3+1/\omega)V}{\pi R^2\left[(1-\beta^2)^{1+\frac{1}{\omega}}-\kappa^{1-\frac{1}{\omega}}(\beta^2-\kappa^2)^{1+\frac{1}{\omega}}\right]}\int_\kappa^\eta\left(\beta^2\frac{1}{\eta}-\eta\right)^{\frac{1}{\omega}}d\eta=-H\int_\kappa^\eta\left(\beta^2\frac{1}{\eta}-\eta\right)^{\frac{1}{\omega}}d\eta,\ \kappa\le\eta\le\beta \tag{6}$$

$$v_b=-\frac{(3+1/\omega)V}{\pi R^2\left[(1-\beta^2)^{1+\frac{1}{\omega}}-\kappa^{1-\frac{1}{\omega}}(\beta^2-\kappa^2)^{1+\frac{1}{\omega}}\right]}\int_\eta^1\left(\eta-\beta^2\frac{1}{\eta}\right)^{\frac{1}{\omega}}d\eta=-H\int_\eta^1\left(\eta-\beta^2\frac{1}{\eta}\right)^{\frac{1}{\omega}}d\eta,\ \beta\le\eta\le 1 \tag{7}$$

and in flow pattern B:

$$v_a=-\left(\frac{3\omega+1}{\omega+1}\right)\frac{V}{\pi(\kappa R)^2}\left(1-\left(\frac{\eta}{\kappa}\right)^{\frac{\omega+1}{\omega}}\right)=-G\left(1-\left(\frac{\eta}{\kappa}\right)^{\frac{\omega+1}{\omega}}\right),\quad 0\le\eta\le\kappa \tag{8}$$

$$v_b=\frac{(3+1/\omega)V}{\pi R^2\left[(1-\beta^2)^{1+\frac{1}{\omega}}-\kappa^{1-\frac{1}{\omega}}(\beta^2-\kappa^2)^{1+\frac{1}{\omega}}\right]}\int_\kappa^\eta\left(\beta^2\frac{1}{\eta}-\eta\right)^{\frac{1}{\omega}}d\eta=H\int_\kappa^\eta\left(\beta^2\frac{1}{\eta}-\eta\right)^{\frac{1}{\omega}}d\eta,\ \kappa\le\eta\le\beta \tag{9}$$

$$v_b=\frac{(3+1/\omega)V}{\pi R^2\left[(1-\beta^2)^{1+\frac{1}{\omega}}-\kappa^{1-\frac{1}{\omega}}(\beta^2-\kappa^2)^{1+\frac{1}{\omega}}\right]}\int_\eta^1\left(\eta-\beta^2\frac{1}{\eta}\right)^{\frac{1}{\omega}}d\eta=H\int_\eta^1\left(\eta-\beta^2\frac{1}{\eta}\right)^{\frac{1}{\omega}}d\eta,\ \beta\le\eta\le 1 \tag{10}$$

The values of β ($v_b(\beta)=v_{b,max}$) in Eq. (6) and Eq. (7) for flow pattern A, and Eq. (9) and Eq. (10) for flow pattern B, were obtained via the given ω and κ, as shown in Table 1 [40]. The terms with the power law index ω on the right-hand side of Eq. (5) and Eq. (6) and (7) for flow pattern A (Eq. (9) and (10) for flow pattern B), respectively, were approximated using the polynomials fitted at the selected points for the acceptable tolerance as follows:

$$\left(1-\left(\frac{\eta_a}{\kappa}\right)^{\frac{\omega+1}{\omega}}\right)=U_1+U_2\eta+U_3\eta^2+U_4\eta^3+U_5\eta^4 \tag{11}$$

$$\int_{\kappa}^{\eta}\left(\beta^2\frac{1}{\eta}-\eta\right)^{\frac{1}{\omega}}d\eta+\int_{\eta}^{1}\left(\eta-\beta^2\frac{1}{\eta}\right)^{\frac{1}{\omega}}d\eta=Z_1+Z_2\eta+Z_3\eta^2+Z_4\eta^3+Z_5\eta^4 \tag{12}$$

Table 1. The values of β in Eqs. (4) and (5) (or Eqs. (7) and (8)) for various ω and κ.

ω \ κ	0.1	0.2	0.3	0.4	0.5	0.6	0.7	0.8	0.9
0.1	0.3442	0.4687	0.5632	0.6431	0.7140	0.7788	0.8389	0.8954	0.9489
0.2	0.3682	0.4856	0.5749	0.6509	0.7191	0.7818	0.8404	0.896	0.9491
0.3	0.3884	0.4991	0.584	0.657	0.7229	0.784	0.8416	0.8965	0.9492
0.4	0.4052	0.5100	0.5912	0.6617	0.7259	0.7858	0.8426	0.8969	0.9493
0.5	0.4193	0.5189	0.597	0.6655	0.7283	0.7872	0.8433	0.8972	0.9493
0.6	0.4312	0.5262	0.6018	0.6686	0.7303	0.7884	0.8439	0.8975	0.9494
0.7	0.4412	0.5324	0.6059	0.6713	0.7319	0.7893	0.8444	0.8977	0.9495
0.8	0.4498	0.5377	0.6093	0.6735	0.7333	0.7902	0.8449	0.8979	0.9495
0.9	0.4872	0.5422	0.6122	0.6754	0.7345	0.7909	0.8452	0.898	0.9495
1.0	0.4637	0.5461	0.6147	0.6770	0.7355	0.7915	0.8455	0.8981	0.9496

The coefficients were obtained with the given power law index $\omega = 0.6$ as an illustration, shown in Table 2.

Table 2. The coefficients in Eqs. (3) and (4) (or Eqs. (7) and (8)) for various κ.

coefficients	$\omega = 0.6$						
κ	0.3	0.5	0.7	κ	0.3	0.5	0.7
U_1	0.4898	0.8694	0.9467	Z_1	-2.4715	-4.3986	-8.5530
U_2	3.2650	0.8362	0.3409	Z_2	17.0332	23.4914	39.6461
U_3	-12.2439	-3.1356	-1.2783	Z_3	-39.9047	-46.0023	-68.7476
U_4	-16.3251	-4.1808	-1.7045	Z_4	39.5577	39.5465	52.9275
U_5	1.0203	0.2613	0.1065	Z_5	-14.2148	-12.6369	-15.2730

The corresponding boundary conditions are:

$$\frac{\partial\varphi_a(0,\xi)}{\partial\eta}=0 \tag{13}$$

$$\frac{\partial\varphi_b(1,\xi)}{\partial\eta}=1+sin(B\xi) \tag{14}$$

$$\frac{\partial\varphi_a(\kappa,\xi)}{\partial\eta}=\frac{\partial\varphi_b(\kappa,\xi)}{\partial\eta} \tag{15}$$

$$\varphi_a(\kappa,\xi)=\varphi_b(\kappa,\xi) \tag{16}$$

in which

$$\eta = \frac{r}{R},\ \kappa = \frac{R_1}{R},\ \xi = \frac{z}{LGz},\ \varphi_a = \frac{k(T_a - T_i)}{q_0'' R}, \varphi_b = \frac{k(T_b - T_i)}{q_0'' R}, B = \beta GzL = 2\pi Gz, Gz = \frac{4V}{\alpha \pi L} \tag{17}$$

The general form of dimensionless temperature distributions of the laminar double-pass countercurrent-flow concentric tube heat exchangers with sinusoidal wall fluxes can be expressed as follows [41]:

$$\varphi_a(\eta, \xi) = \theta_{0a}\xi + \theta_{1a}(\eta) + \theta_{2a}(\eta)\, sin(B\xi) + \theta_{3a}(\eta)\, cos(B\xi) \tag{18}$$

$$\varphi_b(\eta, \xi) = \theta_{0b}\left(\frac{1}{Gz} - \xi\right) + \theta_{1b}(\eta) + \theta_{2b}(\eta)\, sin(B\xi) + \theta_{3b}(\eta)\, cos(B\xi) \tag{19}$$

in which the θ_{0a} and θ_{0b} are the constants yet to be determined, and the $\theta_{1a}(\eta)$, $\theta_{2a}(\eta)$, $\theta_{3a}(\eta)$, $\theta_{1b}(\eta)$, $\theta_{2b}(\eta)$ and $\theta_{3b}(\eta)$ are the functions of η to be determined.

Substituting Eqs. (18) and (19) into the governing equations, Eqs. (3) and (4), and the boundary conditions, Eqs. (13)–(16), yields

$$\begin{aligned}\frac{d}{d\eta}\left(\eta\frac{d\theta_{1a}(\eta)}{d\eta}\right) - \frac{v_a(\eta)R^2\eta}{GzL\alpha}\theta_{0a} + \left[\frac{d}{d\eta}\left(\eta\frac{d\theta_{2a}(\eta)}{d\eta}\right) + \frac{v_a(\eta)BR^2\eta}{GzL\alpha}\theta_{3a}(\eta)\right] sin(B\xi) \\ + \left[\frac{d}{d\eta}\left(\eta\frac{d\theta_{3a}(\eta)}{d\eta}\right) - \frac{v_a(\eta)BR^2\eta}{GzL\alpha}\theta_{2a}(\eta)\right] cos(B\xi) = 0\end{aligned} \tag{20}$$

$$\begin{aligned}\frac{d}{d\eta}\left(\eta\frac{d\theta_{1b}(\eta)}{d\eta}\right) + \frac{v_b(\eta)R^2\eta}{GzL\alpha}\theta_{0b} + \left[\frac{d}{d\eta}\left(\eta\frac{d\theta_{2b}(\eta)}{d\eta}\right) + \frac{v_b(\eta)BR^2\eta}{GzL\alpha}\theta_{3b}(\eta)\right] sin(B\xi) \\ + \left[\frac{d}{d\eta}\left(\eta\frac{d\theta_{3b}(\eta)}{d\eta}\right) - \frac{v_b(\eta)BR^2\eta}{GzL\alpha}\theta_{2b}(\eta)\right] cos(B\xi) = 0\end{aligned} \tag{21}$$

$$\frac{d\theta_{1a}(0)}{d\eta} + \frac{d\theta_{2a}(0)}{d\eta} sin(B\xi) + \frac{d\theta_{3a}(0)}{d\eta} cos(B\xi) = 0 \tag{22}$$

$$\left(\frac{d\theta_{1b}(1)}{d\eta} - 1\right) + \left(\frac{d\theta_{2b}(1)}{d\eta} - 1\right) sin(B\xi) + \left[\frac{d\theta_{3b}(1)}{d\eta}\right] cos(B\xi) = 0 \tag{23}$$

$$\left(\frac{d\theta_{1a}(\kappa)}{d\eta} - \frac{d\theta_{1b}(\kappa)}{d\eta}\right) + \left(\frac{d\theta_{2a}(\kappa)}{d\eta} - \frac{d\theta_{2b}(\kappa)}{d\eta}\right) sin(B\xi) + \left(\frac{d\theta_{3a}(\kappa)}{d\eta} - \frac{d\theta_{3b}(\kappa)}{d\eta}\right) cos(B\xi) = 0 \tag{24}$$

$$\begin{aligned}\theta_{0a}\xi + \theta_{1a}(\kappa) + \theta_{2a}(\kappa)\, sin(B\xi) + \theta_{3a}(\kappa)\, cos(B\xi) \\ = \theta_{0b}\left(\frac{1}{Gz} - \xi\right) + \theta_{1b}(\kappa) + \theta_{2b}(\kappa)\, sin(B\xi) + \theta_{3b}(\kappa)\, cos(B\xi)\end{aligned} \tag{25}$$

2.1. *Solving $\theta_{2a}(\eta)$, $\theta_{3a}(\eta)$, $\theta_{2b}(\eta)$ and $\theta_{3b}(\eta)$by using Frobenius method*

Multiplying Eqs. (20)–(25) by $sin(B\xi)$ and integrating with respect to ξ in the interval [0, $2\pi/B$] gives:

$$\frac{d}{d\eta}\left(\eta\frac{d\theta_{2a}(\eta)}{d\eta}\right)+\frac{v_a(\eta)BR^2\eta}{\alpha GzL}\theta_{3a}(\eta)=0 \tag{26}$$

$$\frac{d}{d\eta}\left(\eta\frac{d\theta_{2b}(\eta)}{d\eta}\right)+\frac{v_b(\eta)BR^2\eta}{\alpha GzL}\theta_{3b}(\eta)=0 \tag{27}$$

$$\frac{d\theta_{2a}(0)}{d\eta}=0 \tag{28}$$

$$\frac{d\theta_{2b}(1)}{d\eta}=1 \tag{29}$$

$$\frac{d\theta_{2a}(\kappa)}{d\eta}=\frac{d\theta_{2b}(\kappa)}{d\eta} \tag{30}$$

$$\theta_{2a}(\kappa)=\theta_{2b}(\kappa) \tag{31}$$

Similarly, multiplying Eqs. (20)–(25) by $cos(B\xi)$ and integrating with respect to ξ in the interval [0, $2\pi/B$], one can obtain:

$$\frac{d}{d\eta}\left(\eta\frac{d\theta_{3a}(\eta)}{d\eta}\right)-\frac{v_a(\eta)BR^2\eta}{\alpha GzL}\theta_{2a}(\eta)=0 \tag{32}$$

$$\frac{d}{d\eta}\left(\eta\frac{d\theta_{3b}(\eta)}{d\eta}\right)-\frac{v_b(\eta)BR^2\eta}{\alpha GzL}\theta_{2b}(\eta)=0 \tag{33}$$

$$\frac{d\theta_{3a}(0)}{d\eta}=0 \tag{34}$$

$$\frac{d\theta_{3b}(1)}{d\eta}=0 \tag{35}$$

$$\frac{d\theta_{3a}(\kappa)}{d\eta}=\frac{d\theta_{3b}(\kappa)}{d\eta} \tag{36}$$

$$\theta_{3a}(\kappa)=\theta_{3b}(\kappa) \tag{37}$$

The complex functions $\psi_a(\eta)=\theta_{2a}(\eta)+\theta_{3a}(\eta)i$ and $\psi_b(\eta)=\theta_{2b}(\eta)+\theta_{3b}(\eta)i$ were introduced to combine Eqs. (26)–(31) and Eqs. (32)–(37) into a unique one-dimensional boundary value problem according to the prior mathematical treatment [41] as follows:

$$\frac{d}{d\eta}\left(\eta\frac{\partial\psi_a(\eta)}{\partial\eta}\right)-\frac{v_a(\eta)BR^2\eta}{GzL\alpha}\psi_a(\eta)\,i=0 \tag{38}$$

$$\frac{d}{d\eta}\left(\eta\frac{\partial\psi_b(\eta)}{\partial\eta}\right)-\frac{v_b(\eta)BR^2\eta}{GzL\alpha}\psi_b(\eta)\,i=0 \tag{39}$$

$$\frac{d\psi_a(0)}{d\eta}=0 \tag{40}$$

$$\frac{d\psi_b(1)}{d\eta}=1 \tag{41}$$

$$\frac{d\psi_a(\kappa)}{d\eta}=\frac{d\psi_b(\kappa)}{d\eta} \tag{42}$$

$$\psi_a(\kappa)=\psi_b(\kappa) \tag{43}$$

We can apply the method of Frobenius which enables one to create a power series solution to solve differential equations. Assuming $\psi_a(\eta)$ and $\psi_b(\eta)$ have the forms of power series multiplied by unknown powers of η, respectively, leads to:

$$\psi_a(\eta)=\sum_{n=0}^{\infty}a_n\eta^{n+r_a},\quad n\geq 0 \tag{44}$$

$$\psi_b(\eta)=\sum_{n=0}^{\infty}b_n\eta^{n+r_b},\quad n\geq 0 \tag{45}$$

One can find the constants of r_a and r_b are proved to be zero in this system equations. The coefficients a_n and b_n are determined by solving Eqs. (38) and (39) and incorporating the boundary conditions of Eqs. (40) to (43), and then comparing with the real and imaginary parts of the complex functions $\psi_a(\eta)=\theta_{2a}(\eta)+\theta_{3a}(\eta)\,i$ and $\psi_b(\eta)=\theta_{2b}(\eta)+\theta_{3b}(\eta)\,i$, and thus the recursive relations were obtained for flow pattern A, respectively, as follows:

$$a_0,\ a_1=0,\ a_n=\frac{BG}{n^2}(U_1a_{n-2}+U_2a_{n-3}+U_3a_{n-4}+U_4a_{n-5}+U_5a_{n-6}),\ n\geq 2 \tag{46}$$

and

$$b_0,\ b_1=0,\ b_n=\frac{-BH}{n^2}(Z_1b_{n-2}+Z_2b_{n-3}+Z_3b_{n-4}+Z_4b_{n-5}+Z_5b_{n-6}),\ n\geq 2 \tag{47}$$

Similarly, the recursive relations of the coefficients a_n and b_n for flow pattern B are

$$a_0,\ a_1=0,\ a_n=\frac{-BG}{n^2}(U_1a_{n-2}+U_2a_{n-3}+U_3a_{n-4}+U_4a_{n-5}+U_5a_{n-6}),\ n\geq 2 \tag{48}$$

and

$$b_0,\ b_1 = 0,\ b_n = \frac{BH}{n^2}(Z_1 b_{n-2} + Z_2 b_{n-3} + Z_3 b_{n-4} + Z_4 b_{n-5} + Z_5 b_{n-6}),\ n \geq 2 \tag{49}$$

2.2. *Solving θ_{0a}, $\theta_{1a}(\eta)$, θ_{0b} and $\theta_{1b}(\eta)$ by double integrations*

Integrations of Eqs. (20) to (25) with respect to ξ in the interval $[0,2\pi/B]$, one can obtain

$$\frac{d}{d\eta}\left(\eta\frac{d\theta_{1a}(\eta)}{d\eta}\right) - \frac{v_a(\eta)R^2\eta}{GzL\alpha}\theta_{0a} = 0 \tag{50}$$

$$\frac{d}{d\eta}\left(\eta\frac{d\theta_{1b}(\eta)}{d\eta}\right) + \frac{v_b(\eta)R^2\eta}{GzL\alpha}\theta_{0b} = 0 \tag{51}$$

$$\frac{d\theta_{1a}(0)}{d\eta} = 0 \tag{52}$$

$$\frac{d\theta_{1b}(1)}{d\eta} = 1 \tag{53}$$

$$\frac{d\theta_{1a}(\kappa)}{d\eta} = \frac{d\theta_{1b}(\kappa)}{d\eta} \tag{54}$$

$$\theta_{0a} = -\theta_{0b} \tag{55}$$

$$\theta_{1a}(\kappa) = \frac{\theta_{0b}}{Gz} + \theta_{1b}(\kappa) \tag{56}$$

Furthermore, integrating Eqs. (50) and (51) twice with respect to η for $\theta_{1a}(\eta)$ and $\theta_{1b}(\eta)$, respectively, yields

$$\theta_{1a} = G\theta_{0a}\left(\frac{1}{4}U_1\eta^2 + \frac{1}{9}U_2\eta^3 + \frac{1}{16}U_3\eta^4 + \frac{1}{25}U_4\eta^5 + \frac{1}{36}U_5\eta^6\right) + \gamma_{1a}\,ln\,\eta + \gamma_{2a} \tag{57}$$

and

$$\theta_{1b} = -H\theta_{0b}\left(\frac{1}{4}Z_1\eta^2 + \frac{1}{9}Z_2\eta^3 + \frac{1}{16}Z_3\eta^4 + \frac{1}{25}Z_4\eta^5 + \frac{1}{36}Z_5\eta^6\right) + \gamma_{1b}\,ln\,\eta + \gamma_{2b} \tag{58}$$

where γ_{1a}, γ_{2a}, γ_{1b} and γ_{2b} are the integrating constants in Eqs. (57) and (58). Since there are six constants (θ_{0a}, θ_{0b}, γ_{1a}, γ_{2a}, γ_{1b} and γ_{2b}) to be determined given five equations (Eqs. (52) to (56)), it needs one extra equation. The additional one equation of the overall energy balance is required as follows:

$$\rho C_p V(T_F - T_i) = \int_0^L q''(z)2\pi R\,dz \tag{59}$$

Eq. (59) can be rewritten as

$$\varphi_F = \int_0^{\frac{1}{Gz}} 8[1 + sin(B\xi)]d\xi = 8\left[\frac{1}{Gz} - \frac{1}{B}\left(cos\left(\frac{B}{Gz}\right) - 1\right)\right] \tag{60}$$

where the φ_F is the average outlet temperature and it is defined as

$$\varphi_F = -\frac{1}{V}\int_{\kappa}^{1} v_b 2\pi R^2 \eta \varphi_b(\eta, 0)d\eta \tag{61}$$

in flow pattern A, and

$$\varphi_F = -\frac{1}{V}\int_{0}^{\kappa} v_a 2\pi R^2 \eta \varphi_a(\eta, 0)d\eta \tag{62}$$

in flow pattern B. Further, Eqs. (61) and (62) should be solved by using Eqs. (6), (7) and (19) and Eqs. (8) and (18) at $\xi = 0$, respectively. Therefore, the complete solutions of dimensionless temperature distributions in a double-pass concentric circular heat exchanger were obtained by substituting the functions of θ_{1a}, θ_{1b}, θ_{2a}, θ_{2b}, θ_{3a} and θ_{3b}, and constants of θ_{0a} and θ_{0b} into the φ_a and φ_b (say Eqs. (18) and (19)).

3. Heat-transfer efficiency enhancement

The local Nusselt number is usually used to measure the convection heat transfer occurring at the wall surface of double-pass concentric circular heat exchangers in forced convection heat-transfer problems and defined as

$$Nu(\xi) = \frac{hDe}{k} \tag{63}$$

where k is the heat conductivity coefficient of the fluid, De is the equivalent diameter of the conduit, $De = 2R$, and h is the heat transfer coefficient. The heat-transfer coefficient h is defined as

$$q_w''(z) = h\big(T_j(R, z) - T_i\big), \text{j} = \text{a,b} \tag{64}$$

or, in the dimensionless form

$$h = \frac{k}{R}\frac{q_w''(\xi)}{q_0''\varphi_j(1, \xi)} = \frac{k}{R}\frac{1 + sin(B\xi)}{\varphi_j(1, \xi)}, \text{j} = \text{a,b} \tag{65}$$

Substituting Eq. (65) into Eq. (63) yields

$$Nu(\xi) = \frac{2[1 + sin(B\xi)]}{\varphi_j(1, \xi)}, \text{j} = \text{a,b} \tag{66}$$

Similarly, the local Nusselt number of single-pass heat exchangers is defined as

$$Nu_0(\xi) = \frac{2[1 + sin(B\xi)]}{\varphi_0(1, \xi)} \tag{67}$$

where the wall temperature distribution, $\varphi_0(1, \xi)$, of single-pass heat exchangers can be determined, according to the reference [41].

Moreover, the average Nusselt numbers of single- and double-pass concentric circular heat

exchangers, respectively, were determined by

$$\overline{Nu} = Gz\int_0^{1/Gz} Nu(\xi)\,d\xi = Gz\int_0^{1/Gz} \frac{2[1+sin(B\xi)]}{\varphi_j(1,\xi)}d\xi, \text{ j = a,b} \tag{68}$$

and

$$\overline{Nu_0} = Gz\int_0^{1/Gz} Nu_0(\xi)\,d\xi = Gz\int_0^{1/Gz} \frac{2[1+sin(B\xi)]}{\varphi_0(1,\xi)}d\xi \tag{69}$$

The heat-transfer efficiency enhancement was illustrated by calculating the percentage increase in the device by employing a double-pass operation, based on single-pass device with the same working dimensions and operating parameters

$$I_h = \frac{\overline{Nu} - \overline{Nu_0}}{\overline{Nu_0}}(\%) \tag{70}$$

4. Power consumption increment

The power consumption increment is unavoidable due to inserting an impermeable sheet into a single-pass device to conduct double-pass operations. The power consumption only incurring the friction losses to walls in double-pass operation were significant. And relations to joint, diversion or bending of conduit are neglected for simplicity. It may be obtained by using generalized Bernoulli equation [42] with following assumptions: (a) incompressible fluid; (b) no change in average velocity; (c) no change in elevation; (d) no work performed. Hence, the power consumption may determine using Fanning friction factor f_F [43]:

$$\ell w_{f,j} = \frac{2f_{F,j}\bar{v}_j^2 L}{De_j}, \quad j = a,b \tag{71}$$

$$P = V\rho\ell w_{f,a} + V\rho\ell w_{f,b}, \;\; P_0 = V\rho\ell w_{f,0} \tag{72}$$

The relative extents I_P of power consumption increment was illustrated by calculating the percentage increment in the double-pass operation, based on the single-pass device as

$$I_P = \frac{P_{\text{double}} - P_{\text{single}}}{P_{\text{single}}} \times 100\% \tag{73}$$

5. Results and discussions

The applications of Frobenius method to solve for differential equations are expanded in terms of an extended power series, say Eqs. (38) and (39). To illustrate, comparison is made to such a power series with terms truncated after $n = 70$ and $n = 75$ with $\kappa = 0.5$ and $\omega = 0.8$. The accuracy of those comparisons is analyzed and some results are presented in Table 3 for an extended power series for flow pattern A. It can be observed from Table 3 that the power series agree reasonably well with the term of $n = 70$, and hence those power series with $n = 70$ are employed in the calculation procedure.

Table 3. The convergence of power series in Eqs. (44) and (45) with $n = 70$ and $n = 75$ for flow pattern A as an illustration.

Gz	n	$\theta_{2a}(0.3)$	$\theta_{3a}(0.3)$	$\theta_{2b}(0.7)$	$\theta_{3b}(0.7)$	$\overline{Nu}$
1	70	-0.092	0.135	0.136	-1.124	0.07
	75	-0.092	0.135	0.136	-1.124	0.07
10	70	-5.2×10^{-24}	-9.2×10^{-23}	1.71×10^{-13}	6.5×10^{-15}	1.87
	75	-6.7×10^{-25}	-2.6×10^{-24}	2.7×10^{-14}	1.0×10^{-15}	1.87
50	70	-1.4×10^{-23}	-7.7×10^{-24}	1.8×10^{-13}	7.2×10^{-15}	6.31
	75	-4.4×10^{-25}	-2.4×10^{-25}	2.8×10^{-14}	1.1×10^{-15}	6.31
100	70	-5.1×10^{-24}	1.7×10^{-24}	1.8×10^{-13}	7.3×10^{-15}	7.92
	75	-1.6×10^{-25}	5.2×10^{-26}	2.8×10^{-14}	-1.1×10^{-15}	7.92
1000	70	-1.3×10^{-38}	-2.3×10^{-38}	1.9×10^{-13}	6.3×10^{-15}	10.06
	75	4.5×10^{-40}	-4.9×10^{-40}	3.0×10^{-14}	1.0×10^{-15}	10.06

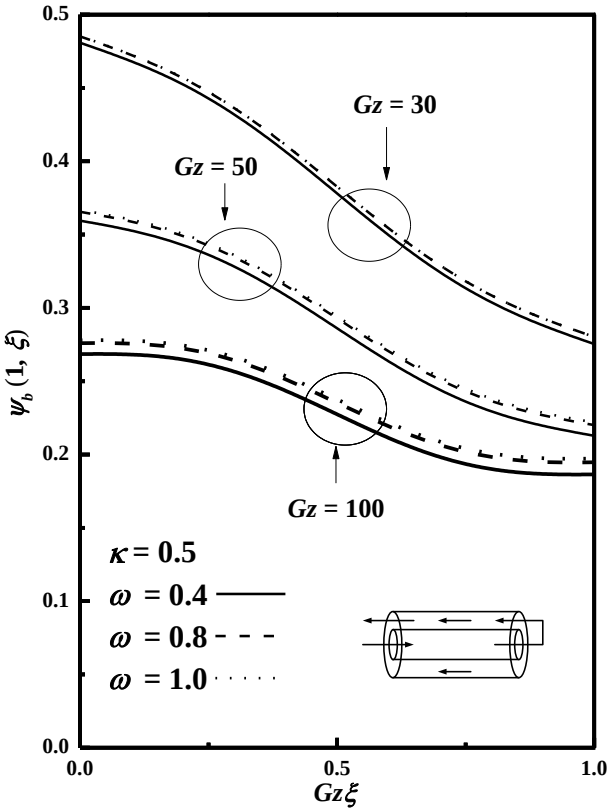

Figure 2. Dimensionless wall temperature distribution with and as parameters (flow pattern A).

The dimensionless temperature distributions of power-law fluids in double-pass concentric circular heat exchanger with sinusoidal wall flux are obtained through solving the energy balance equations with the aid of the linear superposition method. Obtaining the wall temperature distributions in advance of the design of the heat exchanger equipment is important for an engineer to select the appropriate materials and to carefully consider both technical and economic feasibility. It can be observed in Figure 2 for the flow pattern A that the wall temperature is getting lower at the downstream

in subchannel *b*. The wall temperature at the whole part of subchannel *b* could reach an extremely low value, especially for remarkably high flow rate, say Gz =100. On the contrary, the wall temperature is getting higher at the downstream in subchannel *b* for the flow pattern B. The wall temperature profiles are growing up toward the end downstream, as shown in Figure 3 for the flow pattern B. The wall temperatures are found to be close to the inlet temperature at the flow entrance irrespective of the Gz values. The wall temperature becomes a little bit lower for smaller ω (more apparently shear-thinning), regardless of the flow pattern. It is noteworthy that the wall temperatures are monotonically increasing or decreasing along the heat-exchanger device even with the sinusoidal wall heat flux. Regarding the device performance, the simulated Nusselt number Nu is demonstrated in Figure 4, and both flow patterns of the double-pass concentric circular heat exchanger show much more effective energy transfer than that from the single-pass device. The performance of device is further improved along with the increasing Gz. The device with the flow pattern B is shown to be more effective than that of the flow pattern A and single-pass operations under the same ω condtion. For both flow patterns, the Nu is getting lower with the smaller ω.

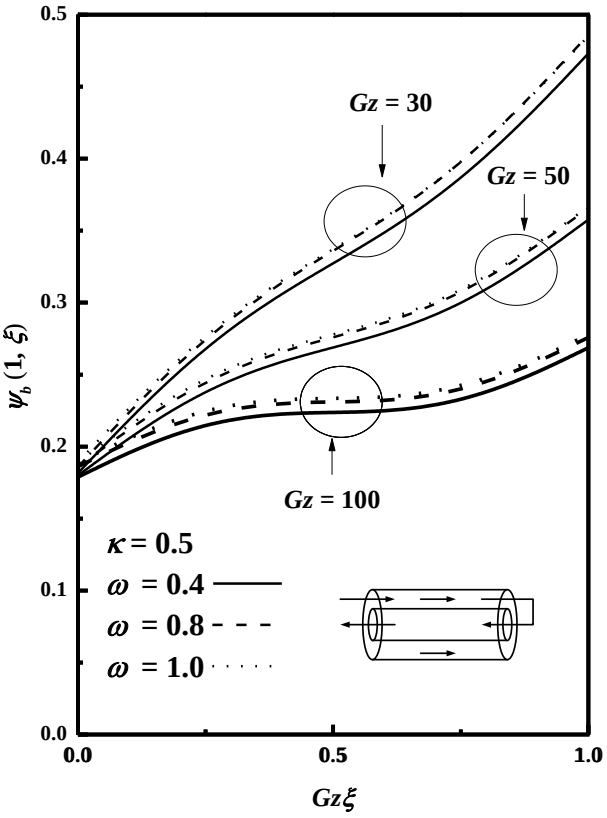

Figure 3. Dimensionless wall temperature distribution with and as parameters (flow pattern B).

The dimensionless wall temperatures are demonstrated in Figures 5 and 6 for the flow patterns A and B, respectively, to illustrate the influence of κvalue (impermeable-sheet position). The wall temperature shows monotonically decreasing tendency for flow pattern A and increasing tendency for flow pattern B. On the other hand, the wall temperature presented longitudinal fluctuations in accordance with the sinusoidal wall flux. It is also found that the wall temperature increases with small κ (relative larger thickness of subchannel *b*) and decrease with a higher Gz for both flow patterns.

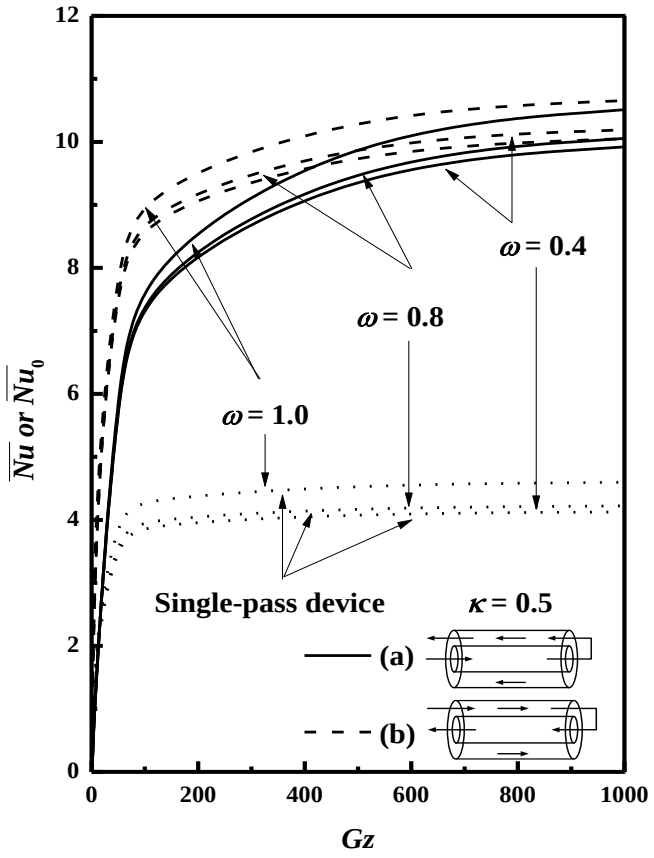

Figure 4. Average Nusselt number vs. Gz with ω as a parameter for κ = 0.5.

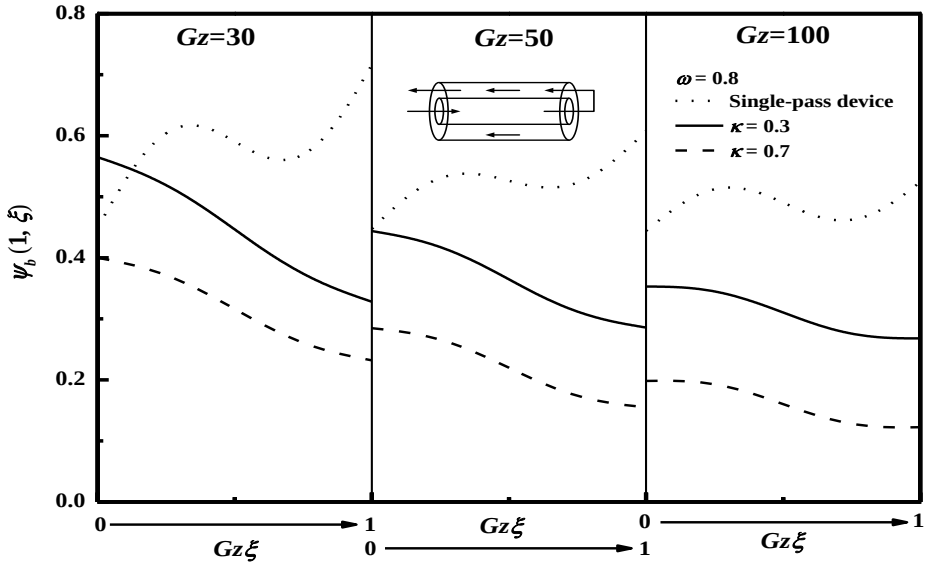

Figure 5. Dimensionless wall temperature vs. $Gz\xi$ with κ for various Gz (flow pattern A).

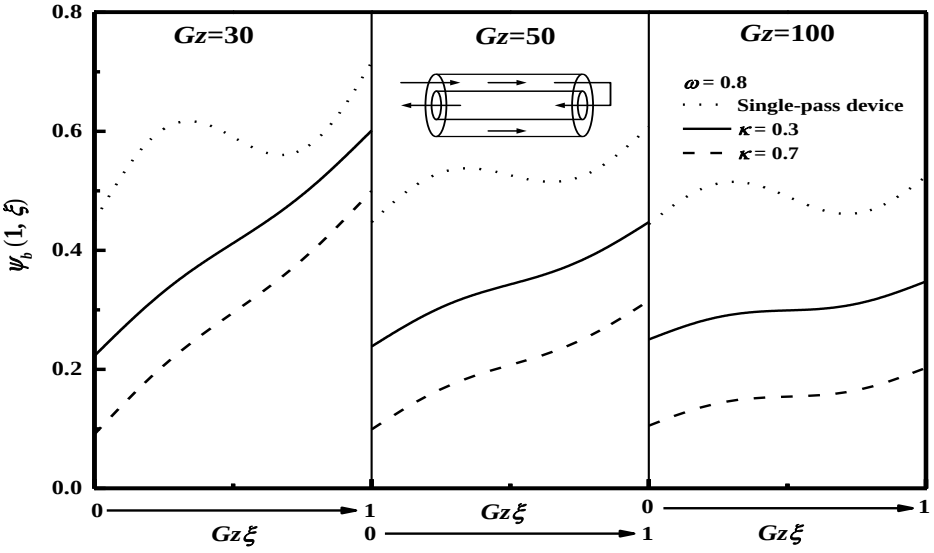

Figure 6. Dimensionless wall temperature vs. $Gz\xi$ with κ for various Gz (flow pattern B).

In Figure 7, it is found that the Nusselt number *Nu* of the current double-pass heat exchanger is sensitive to the κ values. The Nusselt number *Nu* increases with the κ values which indicated the double-pass device with a narrower subchannel *b* could accomplish better heat-transfer efficiency. It is also found the device of flow pattern B could have better device performance improvement than that of flow pattern A.

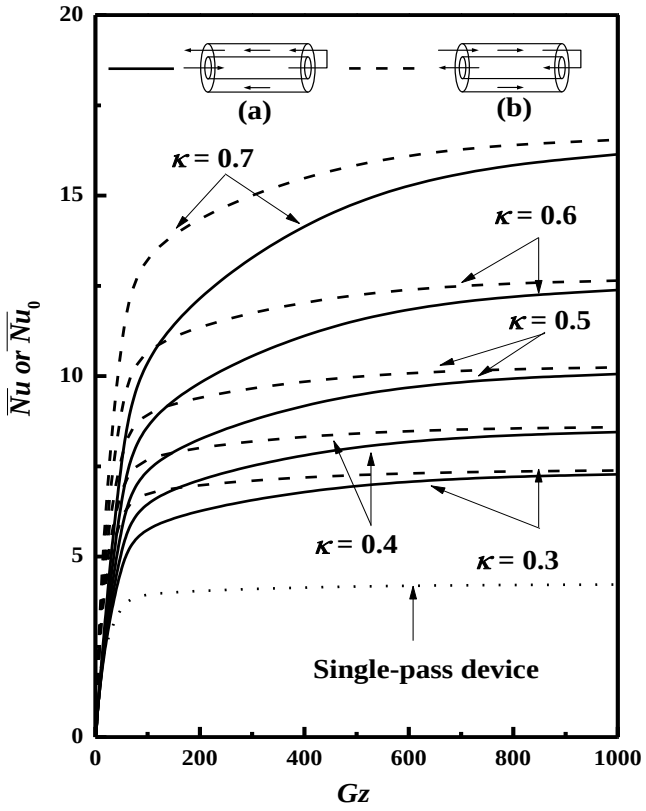

Figure 7. The average Nusselt number vs. Gz with κ as a parameter as a parameter.

When simultaneously considering the heat-transfer improvement enhancement I_h and the power consumption increment I_p, its ratio I_h/I_p is plotted versus Graetz number Gz with the κ value as a parameter in Figure 8 and Tables 4 and 5. The ratio of I_h/I_p rapidly increases with Gz and quickly flatten out. It also rises with the increase in κ. The double-pass device of flow pattern B demonstrated to be more beneficial in economic sense than that of flow pattern A.

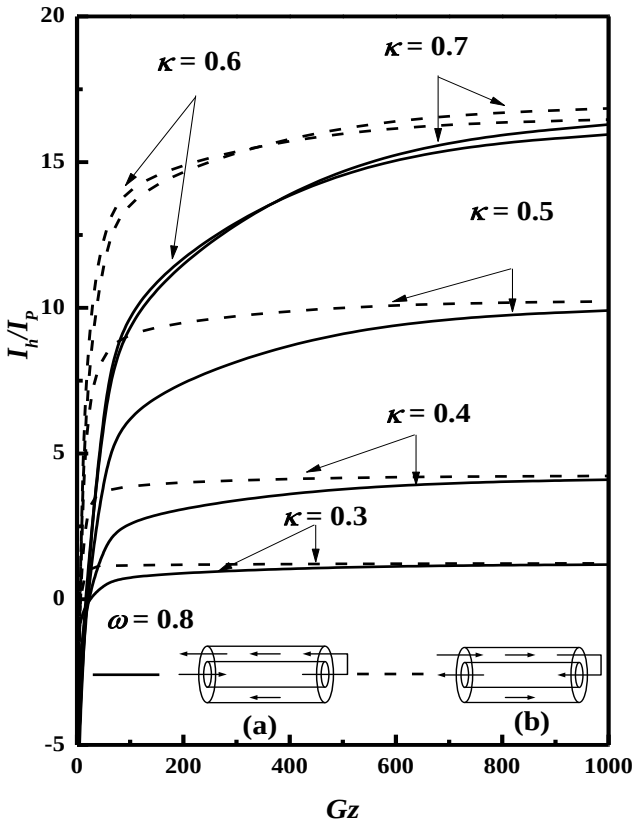

Figure 8. The ratio of I_h/I_p vs. Gz with κ as a parameter.

Table 4. The ratio of I_h/I_p with ω, Gz and κ as parameters for flow pattern A.

I_h/I_p	ω = 0.4			ω = 0.6			ω = 0.8			ω = 1.0		
	Impermeable-sheet position (κ)											
Gz	0.3	0.5	0.7	0.3	0.5	0.7	0.3	0.5	0.7	0.3	0.5	0.7
1	-5.88	-13.68	-11.02	-2.98	-9.34	-7.57	-1.38	-6.38	-5.22	-0.71	-4.31	-3.63
10	-1.36	-3.29	-2.43	-0.60	-2.00	-1.55	-0.25	-1.16	-0.86	-0.1	-0.63	-0.47
100	3.15	13.48	20.48	1.65	9.77	14.74	0.84	6.97	10.58	0.42	4.9	7.55
1000	4.56	19.63	31.99	2.36	14.04	22.98	1.19	9.97	16.29	0.59	6.91	11.56

Table 5. The ratio of I_h/I_p with ω, Gz and κ as parameters for flow pattern B.

I_h/I_p	ω = 0.4			ω = 0.6			ω = 0.8			ω = 1.0		
	Impermeable-sheet position (κ)											
Gz	0.3	0.5	0.7	0.3	0.5	0.7	0.3	0.5	0.7	0.3	0.5	0.7
1	-0.57	-1.29	-1.02	-2.26	-7.08	-5.65	-1.43	-6.43	-5.27	-0.49	-3.01	-2.45
10	4.71	13.58	13.63	2.59	9.43	9.21	1.24	6.6	6.58	0.62	4.71	4.76
100	4.35	18.59	28.29	2.4	13.34	20.15	1.18	9.37	14.28	0.58	6.52	10.12
1000	4.7	20.29	33.16	2.45	14.51	23.79	1.23	10.12	16.84	0.61	7.12	11.94

6. Conclusions

A mathematical formulation for a concentric circular double-pass heat exchanger of power-law fluids with sinusoidal wall flux has been formulated, and the analytical solution is obtained using orthogonal expansion technique. The double-pass flow patterns can be achieved by inserting an impermeable sheet into a cylindrical heat exchanger to examine the heat transfer behavior. The double-pass device performance can be significantly enhanced when compared to that of the single-pass one, especially for a narrower annular flow channel (subchannel b). The average Nusselt number of the device of flow pattern B (annular flow in, core flow out) is larger than that of flow pattern A (core flow in, annular flow out). The longitudinal wall temperature profile is able to be more smoothing despite the sinusoidal wall flux. The wall temperature is decreasing in longitudinal direction for flow pattern A and increasing for flow pattern B, and the variations are much more moderate for high flow rates, for example at Gz = 100. A comparison is also made for the heat-transfer improvement enhancement I_h and the power consumption increment I_p in the form of I_h/I_p. One could find that the flow pattern B always performs better than that of flow pattern A when assessing the economic feasibility of both the flow patterns A and B by ratio I_h/I_p.

Acknowledgments

The authors wish to thank the Ministry of Science and Technology (MOST) of the Republic of China for its financial support.

Conflict of interest

The authors have no conflict of interest.

References

1. R. K. Shah, A. L. London, *Laminar flow forced convection in ducts*, Academic Press, New York, USA, (1978), 196–207.
2. V. D. Dang, M. Steinberg, Convective diffusion with homogeneous and heterogeneous reaction in a tube, *J. Phys. Chem.,* **84** (1980), 214–219.

3. E. Papoutsakis, D. Ramkrishna, Conjugated Graetz problems. I: General formalism and a class of solid-fluid problems, *Chem. Eng. Sci*., **36** (1981), 1381–1390.
4. X. Yin, H. H. Bau, The Conjugated Greatz problem with axial conduction, *Trans. ASME*, **118** (1996), 482–485.
5. R. J. Nunge, W. N. Gill, An analytical study of laminar counterflow double-pipe heat exchangers, *AIChE J.,* **12** (1966), 279–289.
6. G. M. A. Ebadian, H. Y. Zhang, An exact solution of extended Graetz problem with axial heat conduction, *Int. J. Heat Mass Transfer*, **32** (1989), 1709–1717.
7. F. Reyes, W. L. Luyben, Extensions of the simultaneous design of gas-phase adiabatic tubular reactor systems with gas recycle, *Ind. Eng. Chem. Res.*, **40** (2001), 635–647.
8. C. M. C. Bonelli, A. F. Martins, E. B. Mano, C. L. Beatty, Effect of recycled polypropylene on polypropylene/high-density polyethylene blends, *J. Appl. Polym. Sci.*, **80** (2001), 1305–1311.
9. A. Fadavi, Y. Chisti, Gas-liquid mass transfer in a novel forced circulation loop reactor, *Chem. Eng. J.*, **112** (2005), 73–80.
10. M. H. Siegel, J. C. Merchuk, K. Schugerl, Air-Lift Reactor Analysis: Interrelationships between riser, downcomer, and gas-liquid separator behavior including gas recirculation effects, *AIChE J.*, **32** (1986), 1585–1595.
11. K. I. Kikuchi, H. Takahashi, Y. Takeda, F. Sugawara, Hydrodynamic behavior of single particles in a draft-tube bubble column, *Can. J. Chem. Eng.*, **77** (1999), 573–578.
12. C. D. Ho, P. C. Lee, J. W. Tu, Mass transfer enhancement in double-pass parallel-plate mass exchangers under asymmetric wall fluxes, *Chem. Eng. Technol.*, **32** (2009), 1567–1577.
13. C. D. Ho, H. M. Yeh, J. J. Guo, An analytical study on the enrichment of heavy water in the continuous thermal diffusion column with external refluxes, *Sep. Sci. Technol.*, **37** (2002), 3129–3153.
14. C. Heinen, G. Guthausen, H. Buggisch, Determination of the power law exponent from magnetic resonance imaging (MRI) flow data, *Chem. Eng. Technol.*, **25** (2002), 873–877.
15. R. P. Bharti, R. P. Chhabra, V. Eswaran, Steady forced convection heat transfer from a heated circular cylinder to power-law fluids, *Int. J. Heat Mass Transfer*, **50** (2007), 977–990.
16. A. Carezzato, M. R. Alcantara, J. Telis-Romero, C. C. Tadini, J. A. W. Gut, Non-Newtonian heat transfer on a plate heat exchanger with generalized configurations, *Chem. Eng. Technol.*, **32** (2007), 21–26.
17. C. D. Ho, G. G. Lin, W. H. Lan, Analytical and experimental studies of power-law fluids in double-pass heat exchangers for improved device performance under uniform heat fluxes, *Int. J. Heat Mass Transfer*, **61** (2013), 464–474.
18. A. A. Delouei, M. Nazari, M. H. Kayhani, G. Ahmadi, Direct-forcing immersed boundary—non-Newtonian lattice Boltzmann method for transient non-isothermal sedimentation, *J. Aerosol. Sci.*, **104** (2017), 106–122.
19. A. A. Delouei, M. Nazari, M. H. Kayhani, S. K. Kang, S. Succi, Non-Newtonian particulate flow simulation: A direct-forcing immersed boundary–lattice Boltzmann approach, *Phys. A Statist. Mech. Appl.*, **447** (2016), 1–20.
20. A. A. Delouei, M. Nazari, M. H. Kayhani, S. Succi, Non-Newtonian unconfined flow and heat transfer over a heated cylinder using the direct-forcing immersed boundary–thermal lattice Boltzmann method, *Phys. Rev. E*, **89** (2014), 053312.

21. A. Jalali, A. A. Delouei, M. Khorashadizadeh, A. M. Golmohamadi, S. Karimnejad, Mesoscopic simulation of forced convective heat transfer of Carreau-Yasuda fluid flow over an inclined square: Temperature-dependent viscosity, *J. Appl. Comput. Mech.*, **6** (2020), 307–319.
22. A. A. Delouei, M. Nazari, M. H. Kayhani, S. Succi, Immersed boundary—thermal lattice Boltzmann methods for non-newtonian flows over a heated cylinder: A comparative study, *Comm. Comput. Phys.*, **18** (2015), 489–515.
23. A. A. Delouei, M. Nazari, M. H. Kayhani, G. Ahmadi, A non-Newtonian direct numerical study for stationary and moving objects with various shapes: An immersed boundary—Lattice Boltzmann approach, *J. Aerosol Sci.*, **93** (2016), 45–62.
24. V. D. Zimparov, A. K. da Silva, A. Bejan, Thermodynamic optimization of treeshaped flow geometries with constant channel wall temperature, *Int. J. Heat Mass Transfer*, **49** (2006), 4839–4849.
25. B. Weigand, D. Lauffer, The extended Graetz problem with piecewise constant wall temperature for pipe and channel flows, *Int. J. Heat Mass Transfer*, **47** (2004), 5303–5312.
26. A. Behzadmehr, N. Galanis, A. Laneville, Low Reynolds number mixed convection in vertical tubes with uniform wall heat flux, *Int. J. Heat Mass Transfer*, **46** (2003), 4823–4833.
27. O. Manca, S. Nardini, Experimental investigation on natural convection in horizontal channels with the upper wall at uniform heat flux, *Int. J. Heat Mass Transfer*, **50** (2007), 1075–1086.
28. M. Ghalambaz, J. Zhang, Conjugate solid-liquid phase change heat transfer in heatsink filled with phase change material-metal foam, *Int. J. Heat Mass Transfer*, **146** (2020), 118832–118849.
29. M. Ghalambaz, S. M. H. Zadeh, S. A. M. Mehryan, I. Pop, D. S. Wen, Analysis of melting behavior of PCMs in a cavity subject to a non-uniform magnetic field using a moving grid technique, *Appl. Math. Model.*, **77** (2020), 1936–1953.
30. C. J. Ho, Y. C. Liu, M. Ghalambaz, W. M. Yan, Forced convection heat transfer of nano-encapsulated phase change material (NEPCM) suspension in a mini-channel heatsink, *Int. J. Heat Mass Transfer*, **155** (2020), 119858–119870.
31. S. A. M. Mehryan, L. S. Gargari, A. Hajjar, M. Sheremet, Natural convection flow of a suspension containing nano-encapsulated phase change particles in an eccentric annulus, *J. Energy Storage*, **28** (2020), 101236–101273.
32. M. Ghalambaz, S. A. M. Mehryan, A. Hajjar, A. Veismoradi, Unsteady natural convection flow of a suspension comprising nano-encapsulated phase change materials (NEPCMs) in a porous medium, *Adv. Powder Technol.*, **31** (2020), 954–966.
33. C. J. Hsu, Heat transfer in a round tube with sinusoidal wall heat flux distribution, *AIChE J.*, **11** (1965), 690–695.
34. A. Barletta, E. Rossi di Schio, Effects of viscous dissipation on laminar forced convection with axially periodic wall heat flux, *Heat Mass Transfer*, **35** (1999), 9–16.
35. D. K. Choi, D. H. Choi, Developing mixed convection flow in a horizontal tube under circumferentially non-uniform heating, *Int. J. Heat Mass Transfer*, **35** (1994), 1899–1913.
36. D. Y. Lee, S. J. Park, S. T. Ro, Heat transfer by oscillating flow in a circular pipe with a sinusoidal wall temperature distribution, *Int. J. Heat Mass Transfer*, **38** (1995), 2529–2537.
37. C. D. Ho, J. W. Tu, C. M. Yang, Conjugated heat transfer in double-pass laminar counterflow concentric-tube heat exchangers with sinusoidal wall fluxes, *Int. J. Heat Mass Transfer*, **61** (2009), 464–474.
38. D. Murkerjee, E. J. Davis, Direct-contact heat transfer immiscible fluid layers in laminar flow, *AIChE J.*, **18** (1972), 94–101.

39. E. J. Davis, S. Venkatesh, The solution of conjugated multiphase heat and mass transfer problems, *Chem. Eng. J.*, **34** (1979), 775–787.
40. R. W. Hanks, K. M. Larsen, The flow of power-law non-Newtonian fluids in concentric annuli, *Ind. Eng. Chem. Fundam*., **18** (1979), 33–35.
41. A. Barletta, E. Zanchini, Laminar forced convection with sinusoidal wall heat flux distribution: axially periodic regime, *Heat Mass Transfer*, **31** (1995), 41–48.
42. J. O. Wilkes, *Fluid mechanics for chemical engineers*, Prentice-Hall PTR, New Jersey, 1999.
43. J. R. Welty, C. E. Wicks, R. E. Wilson, *Fundamentals of Momentum, Heat, and Mass Transfer*, third ed. John Wiley & Sons, New York, 1984.

Supplementary

Nomenclature

a_n	[-]	constants
B	[m]	constant $B=\beta GzL$
b_n	[-]	constants
De	[m]	hydraulic diameter
f_F	[-]	Fanning friction factor
g_c	[-]	gravity factor
G	[-]	constant
Gz	[-]	Graetz number
H	[-]	constant
h	[kW/mK]	heat transfer coefficient
I_h	[-]	heat-transfer improvement enhancement
I_p	[-]	power consumption increment
k	[kW/mK]	thermal conductivity of the fluid
L	[m]	conduit length
ℓw_f	[kJ/kg]	friction loss in conduit
$\overline{Nu}$	[-]	the average Nusselt number
P	[(Nm)/s]	power consumption
q''	[kW]	wall heat flux
r	[m]	radius coordinate
R	[m]	outer tube radius
R_1	[m]	inter tube radius
T	[K]	temperature of fluid in conduit

U_i	[-]	constants, $i = 1,2,3,4,5$
V	[m^3/s]	inlet volumetric flow rate
v	[m/s]	velocity distribution of fluid
Z_i	[-]	constant, $i = 1,2,3,4,5$
z	[m]	longitudinal coordinate
α	[m^2/s]	thermal diffusivity of fluid
β	[1/m]	constant
$\dot{\gamma}$	[1/s]	shear rate
γ_{1a}, γ_{2a}	[-]	integration constants
γ_{1b}, γ_{2b}	[-]	integration constants
δ	[m]	impermeable sheet thickness
θ	[-]	coefficients
η	[-]	dimensionless radius coordinate, = r/R
κ	[-]	constant = R_1/R
λ	[-]	constant
ξ	[-]	dimensionless longitudinal coordinate = z/GzL
ρ	[kg/m^3]	density of the fluid
τ	[Pa]	shear stress
φ	[-]	dimensionless temperature $k(T - T_i)/q_0''R$
ω	[-]	power-law index
ψ	[-]	complex functions of dimensionless temperature

Subscripts

0	[-] =at the inlet or for the single-pass device
a	[-] =the inner flow channel
b	[-] =the outer flow channel
F	[-] =at the outlet of a double-pass device
i	[-] =at the inlet of a double-pass device
L	[-] =at the end of the channel=
w	[-] =at the wall surface